Sterically Frustrated Aromatic Enes with Various Colors Originating from Multiple Folded and Twisted Conformations in Crystal Polymorphs

Tomohiko Nishiuchi,*[a] Seito Aibara,[a] Takuya Yamakado[b], Ryo Kimura[b], Shohei Saito[b], Hiroyasu Sato[c], and Takashi Kubo*[a,d]

[a]   Dr. T. Nishiuchi, S. Aibara, Prof. Dr. T. Kubo
        Department of Chemistry, Graduate School of Science, Osaka University, 1-1 Machikaneyama, Toyonaka, Osaka 560-0043, Japan
        E-mail: nishiuchit13@chem.sci.osaka-u.ac.jp
[b]   T. Yamakado, R. Kimura, Prof. Dr. S. Saito
        Department of Chemistry, Graduate School of Science, Kyoto University, Kitashirakawa Oiwake, Sakyo, Kyoto 606-8502, Japan
[c]   Dr. H. Sato
        Rigaku Corporation, 3-9-12 Matsubara, Akishima, Tokyo 196-8666, Japan
[d]   Prof. Dr. T. Kubo
        Innovative Catalysis Science Division, Institute for Open and Transdisciplinary Research Initiatives, (ICS-OTRI), Osaka University, Suita, Osaka 565-0871, Japan

        Supporting information for this article is given via a link at the end of the document.

Abstract: Overcrowded ethylenes composed of 10-methyleneanthrone and two bulky aromatic rings contain a twisted carbon-carbon double (C=C) bond as well as a folded anthrone unit. As such, they are unique frustrated aromatic enes (FAEs). Various colored crystals of these FAEs, obtained using different solvents, correspond to multiple metastable conformations of the FAEs with various twist and fold angles of the C=C bond, as well as various dihedral angles of attached aryl units with respect to the C=C bond. The relationships between color and these parameters associated with conformational features around the C=C bond were elucidated using experimental and theoretical studies. Owing to the fact that they are separated by small energy barriers, the variously colored conformations in the FAE crystal change in response to various external stimuli, such as mechanical grinding, hydrostatic pressure and thermal heating.

Introduction

Chromic molecular materials that are stimulus response have attracted increasing interest due their applications in various light, heat, pH, viscosity and mechanical stress sensors.[1] In particular, flexible aromatic π-systems embedded with a movable component, such as cyclooctatetraene (COT)[2,3] or overcrowded ethylene (OCE) moiety,[4,5] have been widely investigated. In these systems, conformations (bent or twisted) of the movable part govern the π-conjugation length of the molecule, which is directly reflected in optical properties (Figure 1). Therefore, to fine control of color change of the chromic behavior, it is necessary to have a properly designed potential energy surface associated with structural changes occurring in ground and excited states, that is, S_0-S_1 gap. For example, bianthorone is a typical OCE in which the ethylene group is part of two aromatic moieties and where steric hindrance is responsible for the existence of a yellow folded and a green twisted conformation.[6] The calculated potential energy profile for interconversion between these conformations (Figure 2) suggests that the process like those of other OCEs has a high activation energy and that it takes place through no isolable intermediates. As a result, the bianthorone undergoes only a single color change between yellow and green in association with this conformational change. On the other hand, if the activation barriers separating several colored conformers are small, a continuous color change might be promoted by a slight energy input, provided by for example weak mechanical stress. In fact, COT based flexible π-systems exhibit this property in the form of a bend angle dependency of its optical properties. However, since small differences in the bent angle of the COT ring have little effect on the optical properties, it is still a challenging task to synthesize molecules whose optical properties are more sensitive to the slight structural changes.
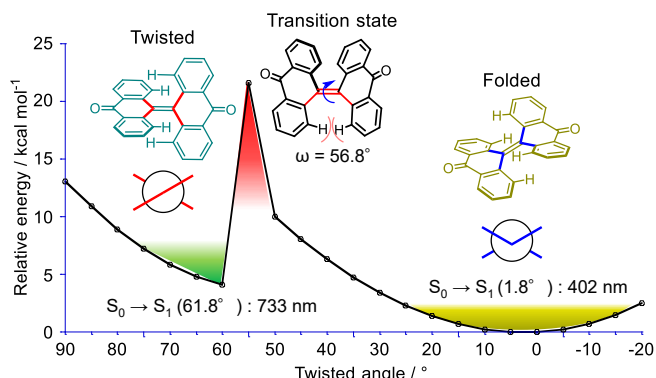
COT embedded flexible π-systems

R¹ = H, R² = -C(=O)N(^{n}Bu)C(=O)-
R¹ = TIPSC≡C, R² = H

OCE embedded π-systems

R = Alkyl or 4-NO$_2$Ph
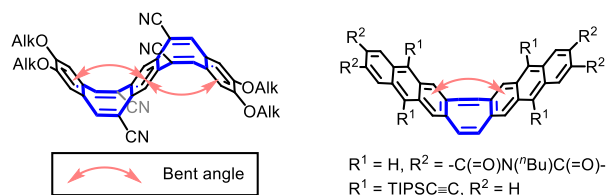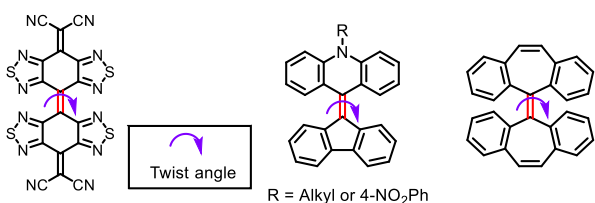
Figure 1. Typical flexible aromatic π-systems embedded within a COT or OCE unit.

Figure 2. Folded and twisted conformations, and transition state structure of bianthrone and potential energies for every 5° of twist angle (ω) together with the calculated S$_0$ → S$_1$ transitions of both the folded (ω = 1.8°) and twisted conformations (ω = 61.8°) calculated using RB3LYP/6-31G*.

The study described below was aimed at developing a strategy to finely control the conformational and optical properties of an OCE using an approach based on the incorporation of multiple moving components. The monotricyclic aromatic ene (MAE, Figure 3a) is known to exist in two conformations differing in the fold and twist of the carbon-carbon double (C=C) bond. The reported twist angle of the is substance is only 7.4° (Figure 3b) and relationships between its conformation and properties, especially optical, have not been well studied.[7] In the current effort, we designed two MAEs that contain a 10-methyleneanthrone moiety and two appended bulky aromatic (9-anthryl or mesityl) rings. The array of groups in these substances cause steric repulsion between the tricyclic anthrone unit and the two bulky aromatic rings, which leads to structural frustration of the C=C bond associated with the formation of conformations having large fold and twist angles (Figure 3c). We have

demonstrated that the sterically frustrated aromatic enes (FAEs) exist in multiple metastable conformations not only having a variety of different fold and twist angles about the C=C bond but also different dihedral angles between the C=C bond and the bulky aromatic rings. The various conformers have close energies in the solid state, and they exhibit unique absorption and emission colors. The relationships that exist between the properties of the conformers and the fold, twist and dihedral angles were elucidated by using experimental and theoretical studies.
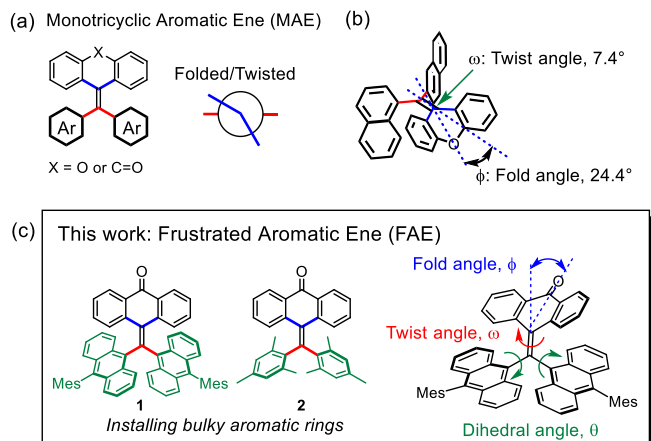

Figure 3. (a) The basic structure of monotricyclic aromatic ene (MAE) with its Newman projection to clarify the fold/twist angles of the C=C bond. (b) First reported MAE composed of xanthene with two naphthyl rings and its fold angle Φ as well as twist angle ω. (c) (left) FAE **1** and FAE **2** possessing a frustrated aromatic ene and (right) identifying twist angle ω, fold angle φ, and dihedral angle θ (right).

Results and Discussion

Conformation-Property Relationships of FAE in the Crystalline State

The method employed to synthesize the bulky aromatic ring containing FAE **1,** using Negishi coupling between 10-(dibromomethylene)-9-anthrone and the substituted anthracenyl zinc chloride, was developed previously.[8] The analogous anthrone derivative FAE **2** was synthesized by using the same procedure (Scheme 1). A study exploring the optical properties of FAE **1** in solution showed that the absorption spectrum is only slightly changed by changing the solvent (Figure S1). FAE **1** was observed to form crystals of various colors in a variety of solvents (Figure 4a). Amber crystals were obtained from acetone (**1**-AO) or dichloromethane-hexane (**1**-DH), orange crystal were generated from DMF (**1**-DMF), red crystals were produced in hexafluorobenzene (**1**-6FB) or 1,1,2,2-tetrachloroethylene (**1**-TCE), and dark red crystals were obtained from acetone (**1**-AD). **1**-AD is a crystal polymorph of **1**-AO. Due to the skeleton of the

OCE, these crystals show aggregation-induced emission (AIE) behavior,[9] and they display various emission colors of amber (**1**-AO and **1**-DH), orange (**1**-DMF), red (**1**-TCE and **1**-6FB) and dark red (**1**-AD). The crystalline-state absorption and emission spectra of the crystals are shown in Figure 4b-e and key spectral data are listed in Table 1.
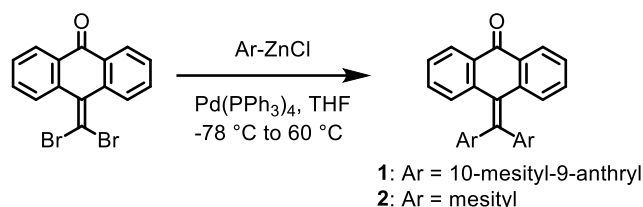
Scheme 1. Route for synthesis of FAE **1** and FAE **2**.

Table 1. Absorption (λ_{abs}) and emission (λ_{em}) wavelengths, and emission quantum yields (Φ_{em}) of **1**-AO, **1**-DH, **1**-DMF, **1**-TCE, **1**-6FB and **1**-AD.

	λ_{abs} / nm[a]	λ_{em} / nm[b]	Φ_{em} / %
1-AO	562	585	23
1-DH	566	585	24
1-DMF	570	596	23
1-TCE	604	620	19
1-6FB	640	605	5
1-AD	657	615, 650(sh)	2

[a] λ_{abs} are onset of absorptions. [b] The λ_{em} are peak maxima.

Even though **1**-AO and **1**-AD were both obtained from acetone their absorption and emission spectra are completely different. Notably, the difference between the absorption onsets (λ_{abs}) of **1**-AO (λ_{abs} = 562 nm) and **1**-AD (λ_{abs} = 657 nm) is 95 nm (2573 cm^{-1}), which is the largest difference observed among the crystals of FAE **1**. The difference in emission maxima (λ_{em}) of these crystals of 65 nm (1710 cm^{-1}) is also the largest in the series. These finding indicate that the color difference between **1**-AO and **1**-AD does not originate from the polarity of recrystallization solvent. Finally, the emission quantum yields of all of the crystals of FAE **1** tend to decrease as their λ_{abs} and λ_{em} are red-shifted.

To gain information about the source(s) of the optical differences, the crystals were subjected to X-ray crystallographic analysis. The conformation of FAE **1** in **1**-AO is shown in Figure 5. As expected, the presence of bulky 9-anthryl units in the FAE **1** skeleton leads not only a large fold angle for the C=C bond (φ = 31.5°) but also a large twist angle of the C=C bond (ω = 25.9°).

Inspection of the crystallographic data for the other crystals (Figure S3-S7) showed that both the fold and twist angles vary as do the dihedral angles θ between the C=C bond and two anthracenyl units. In addition, intermolecular interactions were found to exist between anthrone units in neighboring FAE **1** molecules in **1**-AO. However, the interactions only occur at edge position with distances of 3.54 Å (O···O) and 3.44 Å (C···C) (Figure 5c). Anthrone-anthrone interactions were also seen in the other crystals except **1**-6FB, and the arrangement was different in each.

With the crystallographic data for the crystals of FAE **1** in hand, we next assessed whether a rational relationship exists between the conformational and optical properties. The key structural and conformational parameters, such as C=C bond length, C=O bond length in the anthrone unit, twist angle ω and fold angle φ of the C=C bond, and dihedral angle θ of 9-anthryl units are accumulated in Table 2. Although the C=C and C=O bond lengths were expected to depend on λ_{abs} and λ_{em} values for the crystals, a correlation between does not exist. IR peak positions for C=O vibrations were determined and again no correlation was found between them and the optical properties (Figure S10).

Table 2. Parameters for conformational features around C=C bond of FAE **1. In each crystal**: C=C bond length (Å), C=O bond length (Å) in the anthrone unit, twist angle ω (°) of C=C bond, fold angle φ (°) of C=C bond, and dihedral angle θ (°) of anthracenyl units.

	C=C / Å	C=O / Å	ω / °	φ / °	θ / °
1-AO	1.379	1.222	25.9	31.5	53.6, 67.7
1-DH	1.365	1.224	26.3	30.7	53.4, 66.1
1-DMF	1.374	1.214	26.9	30.0	50.4, 64.8
1-TCE	1.380	1.227	27.3	30.7	53.0, 62.0
1-6FB	1.379	1.223	31.4	26.7	50.2, 59.0
1-AD	1.387	1.230	29.5	25.5	51.0, 52.9

In contrast, we found that trends do exist in the ω, φ and θ values and that they correlate with the optical properties. Specifically, as the twist angle ω increases, the absorption onset and emission maximum shift to longer wavelength. Furthermore, the fold angles φ for FAE **1** in the red and dark red crystals **1**-6FB and **1**-AD, (23.3°, 26.7° and 25.5°, respectively) are smaller than those of the amber and orange crystals (**1**-AO: 31.5°, **1**-DH: 30.7°, **1**-DMF: 30.0°, and **1**-TCE: 30.7°).
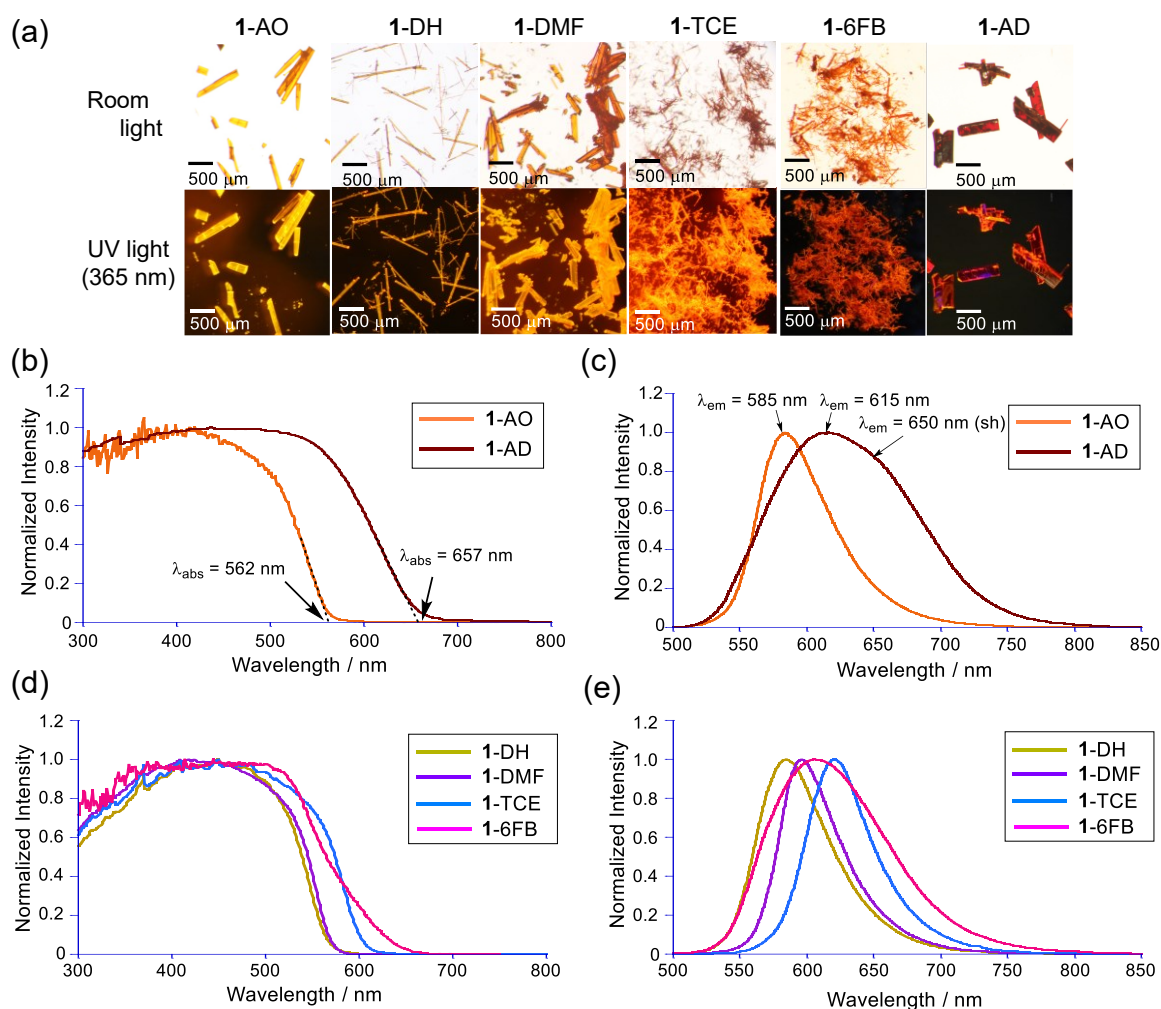
Figure 4. (a) Photoimages of various cyrtal colors of FAE **1** (**1**-AO, **1**-DH, **1**-DMF, **1**-TCE, **1**-6FB, and **1**-AD,) under room light and UV light (365 nm). (b) Crystalline-state diffuse-reflection absorption spectra of **1**-AO and **1**-AD. (c) Crystalline-state emission spectra of **1**-AO and **1**-AD. (d) Crystalline-state diffuse-reflection absorption spectra of **1**-DH, **1**-DMF, **1**-TCE, and **1**-6FB. (e) Crystalline-state emission spectra of **1**-DH, **1**-DMF, **1**-TCE, and **1**-6FB.
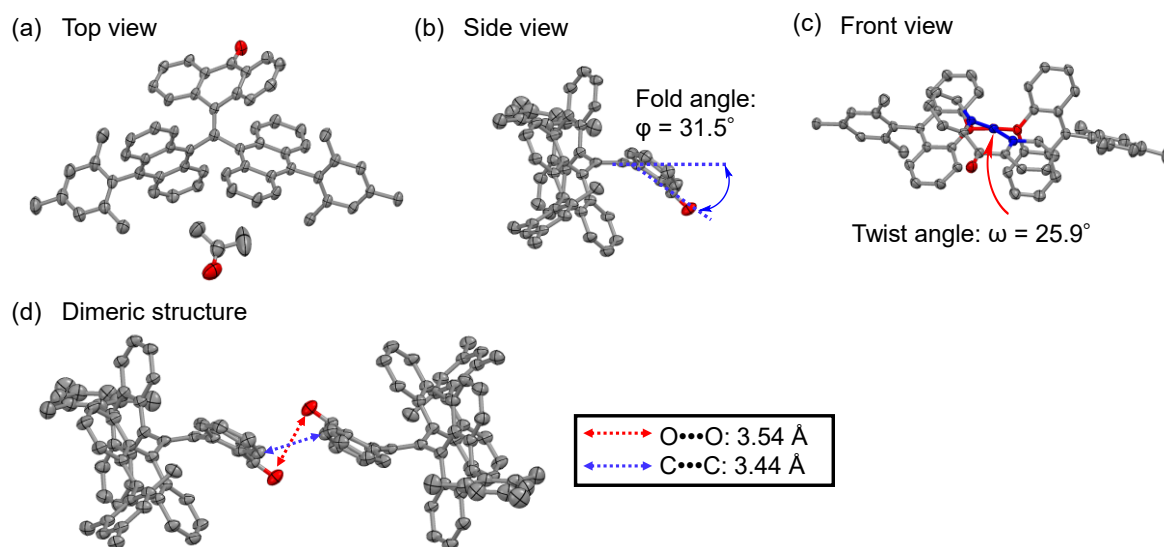

Figure 5. The molecular structure of FAE **1** in **1**-AO. (a) Top view (together with a recrystallized aceton molecule). (b) Side view with folded angle of C=C bond. (c) Front view with twisted angle of C=C bond. (d) Intermolecular contact at the edge of anthrone unit with neighbored molecule. Protons are omitted for clarity.

4

To gain more information about the relationship between these angles and the optical properties, TD-DFT calculations of conformations of FAE **1** with different twist and fold angles of the C=C bond were conducted (Figure S12, S13). In Figure 6 is given a 3D map of TD-DFT results (x-axis: twisted angle ω, y-axis: folded angle φ, z-axis: $S_0 \rightarrow S_1$ transition). Inspection of the map shows that a longer wavelength shift in the $S_0 \rightarrow S_1$ transition takes place not only as the twist angle increases but also as the fold decreases. This finding is in good agreement with the experimental results. Within the range of the simulated fold and twist angles, distributions of the HOMO and LUMO orbitals of FAE **1** slightly expand with increasing twist angle, but they do not significantly change (Figure S14). It is noteworthy that calculated potential energy (PE) differences between the conformation corresponding to the shortest absorption wavelength at 517 nm (ω = 25°, φ = 30°) and to that of the longest wavelength at 637 nm (ω = 45°, φ = 15°) is only 4.41 kcal mol^{-1} (Figure S15). In addition, the PE in S_1 state is greatly stabilized by increasing twist angle and decreasing fold angle, showing the opposite trend to that in the S_0 state (Figure S16). This finding suggests that a significant absorption wavelength change is triggered by only a slight conformational change in the solid state.

Analysis of the data indicates that dihedral angle θ is also an important factor governing optical properties. Comparison of the conformations of FAE **1** in crystals between **1**-6FB and **1**-AD shows that, although the absorption and emission properties are totally different, only a small difference exists in the twist and fold angles, but a significant difference is present in the dihedral angles. The dihedral angles θ of **1**-6FB are 50.2° and 59.0°, respectively, while those of **1**-AD are 51.0° and 52.9°. TD-DFT calculations indicate that decreasing the dihedral angle of FAE **1**, with fixed twist and fold angles leads to a longer wavelength shift in the absorption onset (Figure S17). Moreover, TD-DFT calculations on the monomer structures of FAE **1** in **1**-6FB and **1**-AD show that the $S_0 \rightarrow S_1$ transition of **1**-AD (573 nm) occurs at longer wavelength than that of **1**-6FB (531 nm) (Table S1). Therefore, the optical differences between **1**-6FB and **1**-AD are mainly due to a difference in their dihedral angles.

The crystallographic data for **1**-DMF and **1**-TCE provide further information about factors that govern optical properties of FAE **1**. No significant differences exist in the ω, φ and θ values of **1**-DMF and **1**-TCE, yet their absorption and emission spectra differ. Inspection of the crystal packing structures shows that the anthrone unit in **1**-TCE engages in significant intermolecular π-π interaction with the anthrone unit of a neighboring molecule, while no anthrone-anthrone π-π interaction occurs in **1**-DMF (Figure S4, S5). TD-DFT calculations were carried out on monomeric and
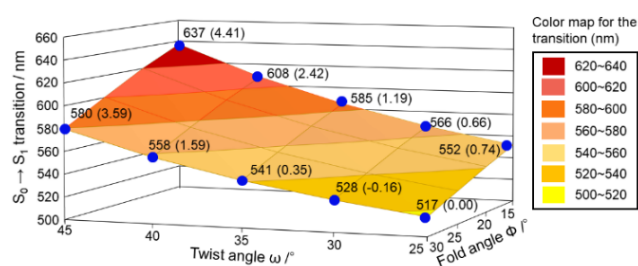
**Figure 6**. 3D map of TD-DFT calculated results (B3LYP/6-31G*//B3LYP/6-31G*) of FAE **1** (x-axis: twist angle ω from 25° to 45°, y-axis: fold angle φ from 15° to 30°, z-axis: $S_0 \rightarrow S_1$ transition). The numbers near the blue dots on the 3D map surface indicate the $S_0 \rightarrow S_1$ transition at the position, and the numbers in parentheses indicate the relative potential energy at the position (kcal mol^{-1}, the referring structure is ω = 25°, φ = 30°, calculated by B3LYP/6-31G*).

dimeric structures. The results indicate that the $S_0 \rightarrow S_1$ transition of the monomeric structure of **1**-TCE occurs at 524 nm, which is a longer wavelength than that of monomeric **1**-DMF (509 nm). Moreover, the dimeric structure of **1**-TCE, having large π-π overlap between the anthrone units, has longer wavelength $S_0 \rightarrow S_1$ transition at 531 nm, whereas that of dimeric structure of **1**-DMF is at 509 nm (Table S1). Thus, although the effect of the intermolecular π-π interaction between the anthrone units cannot exclude as a factor affecting the color difference between **1**-DMF and **1**-TCE,[10] it can be concluded that the main contribution for the various colors in these crystals is the slight structural difference around the frustrated aromatic C=C bond.

To gain further information, the optical properties of FAE **2** in the crystalline state were determined. Different from FAE **1**, FAE **2** generates only two crystal polymorphs that do not contain co-cystallization solvent and exhibit yellow (**2**-Y) and orange (**2**-O) colors (Figure 7a). The respective UV-vis and emission wavelengths of **2**-Y are λ_{abs} = 515 nm and λ_{em} = 555 nm and it has a relatively high emission quantum yield of 32%. In contrast, **2**-O has λ_{abs} = 560 nm and λ_{em} = 610 nm along with a low emission quantum yield of 1% (Figure 7b-c). X-ray crystallographic analysis shows that **2**-O is comprised of two independent conformations **2**-O-a and **2**-O-b, while only one conformation exists for **2**-Y (Figure 8). The key parameters around the frustrated C=C bond are listed in Table 3. TD-DFT calculations show that the $S_0 \rightarrow S_1$ transition of **2**-O-a is estimated to occur at 398 nm, which is shorter than that of **2**-Y (411 nm), owing likely to the existence of a large fold angle φ in the latter (**2**-Y: 20.4°, **2**-O-a: 29.7°) (Figure S18, Table S2). On the other hand, **2**-O-b has a larger twist angle (ω = 26.3°), smaller fold angle (φ = 24.1°) and smaller dihedral angles (θ = 51.6° and 59.9°) than does **2**-O-a. These factors cause the calculated $S_0 \rightarrow S_1$ transition of **2**-O-a to take place at 419 nm. The experimental and theoretical results arising from studies of FAE **2** are consistent with those coming from FAE **1**. Although an anthrone-anthrone interaction is present in **2**-O, TD-DFT calculations show that its effect on the absorption wavelength is

relatively small, which is identical to the tendency seen with FAE **1**.
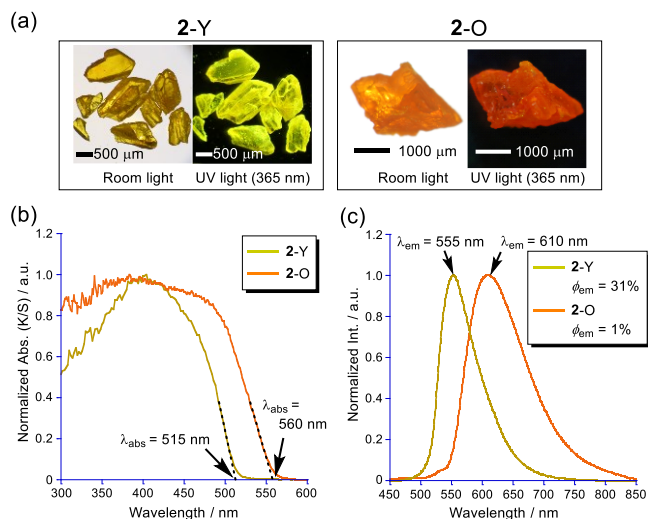
Figure 7. (a) Photoimages of the cyrstals **2**-Y (left) and **2**-O (right) under room light and UV light (365 nm). (b) Crystalline-state diffuse-reflection absorption spectra of **2**-Y and **2**-O. (c) Crystalline-state emission spectra and emission quantum yields of **2**-Y and **2**-O.
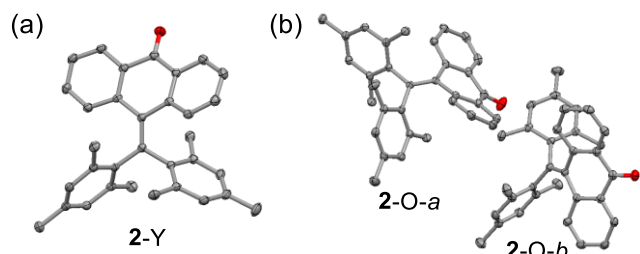
Figure 8. (a) Conformation of FAE **2** in **2**-Y. (b) Conformation of FAE **2** in **2**-O. Two independent conformations **2**-O-*a* and **2**-O-*b* are observed. Protons are omitted for clarity.

Table 3. Parameters for conformational features around the C=C bond of FAE **2**: C=C bond length (Å), C=O bond length (Å) in the anthrone unit, twist angle ω (°) of C=C bond, fold angle φ (°) of C=C bond, and dihedral angle θ (°) of anthracenyl units.

|	C=C / Å	C=O / Å	ω / °	φ / °	θ / °
2-Y	1.377	1.230	19.3	20.4	57.8, 62.2
2-O-*a*	1.370	1.223	22.4	29.7	51.5, 63.5
2-O-*b*	1.380	1.231	26.3	24.1	51.6, 59.9

Mechano-, Piezo-, and Thermochromism of FAE skeleton

Similar to those of other OCEs, FAE **1** and **2** display mechanochromic behavior in the solid state.[4f-h, 11] For example, grinding an orange crystal of FAE **1** or yellow crystal of FAE **2**

causes the colors to change to dark red and orange color, respectively (Figure 9, Figure S19). The color changes take place synchronously with a red-shift in the emission bands as well as a reduction in emission quantum yields (Figure 10). These changes are a consequence of alterations occurring in the parameters associated with conformational features surrounding the frustrated C=C bond as was discussed above.

Because crystal **2**-Y has a large crystal size and it does not contain a co-crystallization solvent, it is suitable for investigating how structural changes occur under application of hydrostatic pressure.[12] When hydrostatic pressure was applied to **2**-Y using a diamond anvil cell (DAC), the crystal color changed from yellow to amber (Figure 11a). The emission maximum underwent a corresponding red-shift from 555 nm to 565 nm (Figure 11b, Figure S20), which is similar to the change taking place when it is ground. Single crystal X-ray measurements made after applying hydrostatic pressure at 3.5 GPa revealed that the color change does not originate from an increase in twist angle ω but rather to flattening of the fold angle φ (Figure 11c, Figure S21). Specifically, the twist angle ω decreases from 20.0° to 15.8° and the fold angle φ also decreases from 21.1° to 12.4°. TD-DFT calculations support the proposal that this conformational change leads to a red-shift of the $S_0 \rightarrow S_1$ transition from 392 nm (0 GPa) to 400 nm (3.5 GPa). Thus, this result indicates that the red-shift associated mechanochromism of FAE **1** and **2** is not solely due to an increase in the twist angle of the C=C bond.
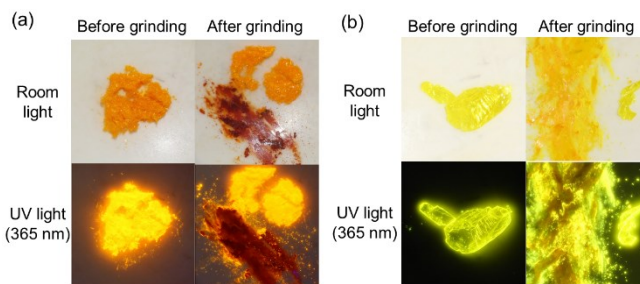

Figure 9. Images before and after grinding (a) **1**-DH and (b) **2**-Y under room and UV light (365 nm).
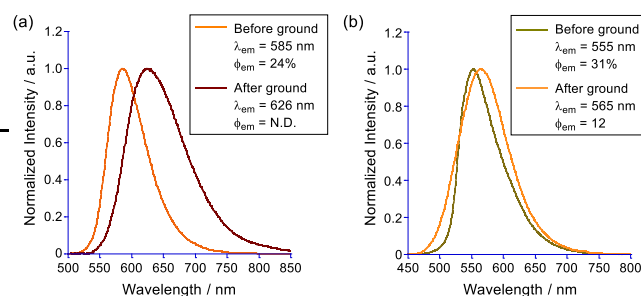
Figure 10. (a) Emission spectra before and after grinding **1**-DH. (b) Emission spectra of before and after grinding **2**-Y.

6
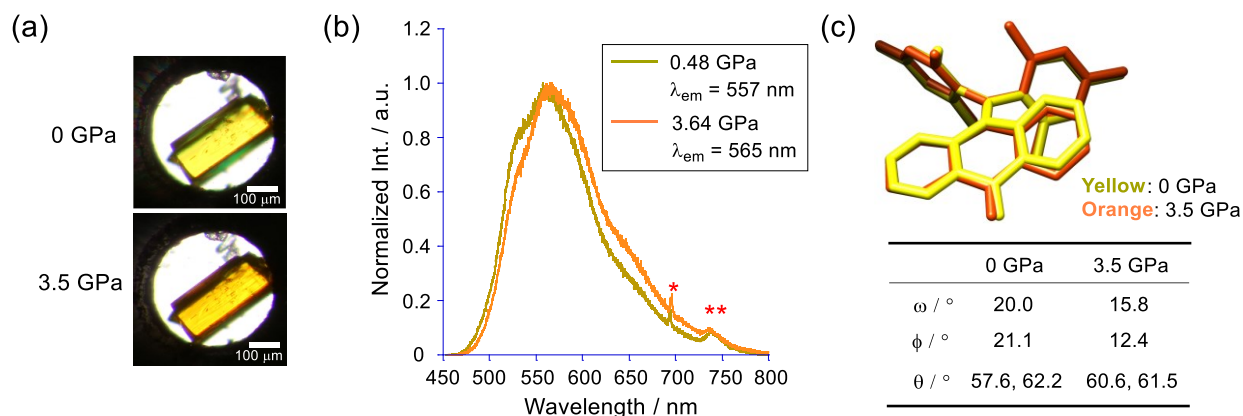
Figure 11. (a) Photoimages of **2**-Y before (top) and after applying hydrostatic pressure with 3.5 GPa (down). (b) Emission spectra of **2**-Y under 0.48 GPa (yellow line) and 3.64 GPa (orange line). Red * indicates the emission from ruby. Red ** indicates the second-order diffraction of excitation light (λ_{ex} = 370 nm). (c) Superposition of the X-ray crystalographic structures of **2**-Y generated by before (0 GPa: yellow) and after applying hydrostatic pressure (3.5 GPa: orange).
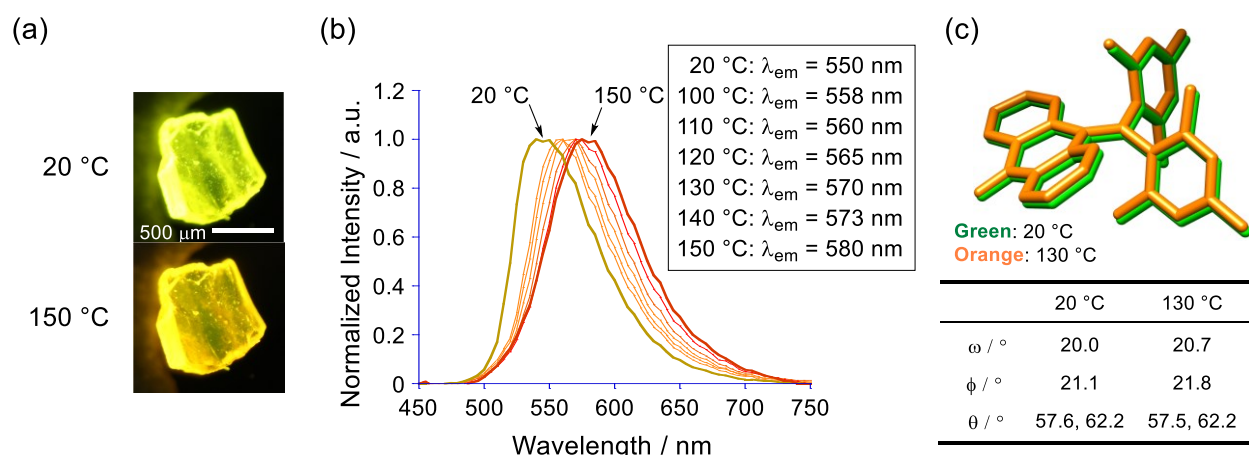
Figure 12. (a) Photoimages of **2**-Y at 20 °C (top) and 150 °C (down) under UV light (365 nm). (b) Emission spectra of **2**-Y at 20 °C (yellow) to 150 °C (dark red) and emission peak tops λ_{em} at each temperature. (c) Superposition of the X-ray crystalographic structures of **2**-Y at 20 °C (green) and 130 °C (orange).

Further efforts showed that crystal **2**-Y exhibits thermochromic fluorescence behavior as well.[2b,13] Upon heating **2**-Y over 100 °C, the fluorescence color gradually changes from yellow to orange and returned to yellow upon cooling (Figure 12a, Figure S22). The emission peak λ_{em} = 550 nm at 20°C is clearly red-shifted to 580 nm at 150°C (Figure 12b), and the half-width of the emission band increases with an increase in temperature from 20 °C (520~590 nm, 2280 cm^{-1}) to 150 °C (545~625 nm, 2350 cm^{-1}). Interestingly, a comparison of the X-ray crystallographic data for **2**-Y at 20 °C and 130 °C[14] (Figure 12c) shows that no significant changes occur in the parameters related to conformation features around the frustrated C=C bond. Rather, only a slight elongation of intermolecular distances takes place by heating, which results in an expansion of the void volume in a unit cell from 330 Å^3 to 386 Å^3 (Figure S23).[15]

TD-DFT calculations were conducted to estimate the lowest energy excited state conformation of FAE **2**. The results show that the excited state of FAE **2** has a propeller shape with the twist angle ω = 59.5°, fold angle φ = 0° and dihedral angle θ = 40.7°

(Figure S24). Therefore, a plausible explanation for the thermochromic fluorescence behavior of **2**-Y associated with red-shifted emission at high temperatures is that structural relaxation occurs through reduction of intermolecular interactions and expansion of the void volume to accommodate the twisted structure of the excited state.[16] Furthermore, the lack of thermochromic fluorescence behavior of **2**-O even though an identical tendency to expand the void volume in a unit cell occurs at high temperature (Figure S25,S26, Table S3). The difference is probably a consequence of intermolecular anthrone-anthrone interactions present **2**-O that interfere with conformational relaxation enabling accommodation of the twisted structure of the excited state.

Conclusion

In the investigation described above, information was gained about relationships that exist between the conformational and optical properties of the crystal states of sterically frustrated

aromatic enes (FAEs). We demonstrated experimentally and theoretically that FAE **1** and FAE **2** form various color crystals, that correspond to multiple metastable conformations with various twist and fold angles of the C=C bond, as well as various dihedral angles of attached aryl units with the C=C bond. Different from usual OCEs exhibiting only folded and twisted forms separated by large energy gaps and/or large activation energies, the FAEs possess conformational energy profiles in which multi-colored crystal polymorph with a variety of different fold, twist and dihedral angles exist as metastable intermediates. In addition, conformational/color changes of the FAE crystals can be readily induced by external stimuli such as mechanical grinding, hydrostatic pressure and thermal heating. We anticipate that the multi-chromic properties associated with slight conformational changes make the FAEs appropriate candidates for multipurpose sensors that can be utilized to detect small energy loads in artificial or biological materials.[17]

Keywords: overcrowded ethylene• Metastable structures • Mechanochromism • Piezochromism •Thermochromism

[1]   Typical reviews for chromic molecules, see: a) C. Reichardt, *Chem. Soc. Rev.* **1992**, *21*, 147.; b) E. Hadjoudis, I. M. Mavridis, *Chem. Soc. Rev.* **2004**, *33*, 579.; b) M. Irie, T. Fukaminato, K. Matsuda, S. Kobatake, *Chem. Rev.* **2014**, *114*, 12174.; c) D. Bléger, S. Hecht, *Angew. Chem. Int. Ed.* **2015**, *54*, 11338.; d) A. Fihey, A. Perrier, W. R. Browne, D. Jacquemin, *Chem. Soc. Rev.* **2015**, *44*, 3719.; d) M. A. Haidekker, E. A. Theodorakis, *J. Mater. Chem. C.* **2016**, *4*, 2707.; e) M K. Kuimova, *Phys. Chem. Chem. Phys.* **2012**, *14*, 12671.; f) Z. Yang, J. Cao, Y. He, J. H. Yang, T. Kim, X. Peng, J. S. Kim, *Chem.Soc. Rev.* **2014**, *43*, 4563.; g) T. Kowada, H. Maeda, K. Kikuchi, *Chem. Soc. Rev*, **2015**, *44*, 4953.

[2]   a) T. Nishiuchi, Y. Kuwatani, T. Nishinaga, M. Iyoda, *Chem. Eur. J.* **2009**, *15*, 6838.; b) T. Nishiuchi, K. Tanaka, Y. Kuwatani, J. Sung, T. Nishinaga, D. Kim, M. Iyoda, *Chem. Eur. J.* **2013**, *19*, 4110.; c) T. Nishiuchi, M. Iyoda,

Bull. Chem. Soc. Jpn. **2014**, *87*, 960.; d) T. Nishiuchi, M. Iyoda, *Chem. Rec.* **2015**, *15*, 329.

[3]   a) C. Yuan, S. Saito, C. Camacho, S. Irle, I. Hisaki, S. Yamaguchi, *J. Am. Chem. Soc.* **2013**, *135*, 8842.; b) C. Yuan, S. Saito, C. Camacho, T. Kowalczyk, S. Irle, S. Yamaguchi, *Chem. Eur. J.* **2014**, *20*, 2193.; c) S. Saito, S. Nobusue, E. Tsuzaka, C. Yuan, C. Mori, M. Hara, T. Seki, C. Camacho, S. Irle, S. Yamaguchi, *Nat. Commun.* **2016**, *7*, 12094.; d) R. Kotani, H. Sotome, H. Okajima, S. Yokoyama, Y. Nakaike, A. Kashiwagi, C. Mori, Y. Nakada, S. Yamaguchi, A. Otsuka, A. Sakamoto, H. Miyasaka, S. Saito, *J. Mater. Chem. C.* **2017**, *5*, 5248.; e) T. Yamakado, K. Otsubo, A. Osuka, S. Saito, *J. Am. Chem. Soc.* **2018**, *140*, 6245.; f) R. Kimura, H. Kuramochi, P. Liu, T. Yamakado, A. Osuka, T. Tahara, S. Saito, *Angew. Chem. Int. Ed.* **2020**, *59*, 16430.

[4]   Typical examples of OCEs composed of bistricyclic aromatic ene skeleton, see: a) I. Agranat, M. R. Suissa, *Struct. Chem.* **1993**, *4*, 59.; b) T. Suzuki, T. Fukushima, T. Miyashi, T. Tsuji, *Angew. Chem. Int. Ed. Engl.* **1997**, *36*, 2495.; c) P. U. Biedermann, J. J. Stezowski, I. Agranate, *Chem. Eur. J.* **2006**, *12*, 3345.; d) C. Wentrup, M. J. Regimbald-Krnel, D. Müller, P. Comba, *Angew. Chem. Int. Ed.* **2016**, *55*, 14600.;.e) A. Takai, D. J. Freas, T. Suzuki, M. Sugimoto, J. Labuta, R. Haruki, R. Kumai, S-i. Aadachi, H. Sakai, T. Hasobe, Y. Matsushita, M. Takeuchi, *Org. Chem. Front.* **2017**, *4*, 650.; f) T. Suzuki, H. Okada, T. Nakagawa, K. Komatsu, C. Fujimoto, H. Kagi, Y. Matsuo, *Chem. Sci.* **2018**, *9*, 475.; g) Y. Matsuo, Y. Wang, H. Ueno, T. Nakagawa, H. Okada, *Angew. Chem. Int. Ed.* **2019**, *58*, 8762.; h) Y. Wang, Y. Ma, K. Ogumi, B. Wang, T. Nakagawa, Y. Fu, Y. Matsuo, *Commun. Chem.* **2020**, *3*, 93.; i) Y. Adachi, Y. Nomura, S. Tazuhara, H. Naito, J. Ohshita, *Chem. Commun.* **2021**, *57*, 1316.

[5]   Typical examples of recent OCEs composed of anthraquinodimethane core, see: a) X. Zhang, X. Jiang, K. Zhang, L. Mao, J. Luo, C. Chi, H. S. O. Chan, J. Wu, *J. Org. Chem.* **2010**, *75*, 8069.; b) T. Suzuki, Y. Ishigaki, K. Sugawara, Y. Umezawa, R. Katoono, A. Shimoyama, Y. Manabe, K. Fukase, T. Fukushima, *Tetrahedron* **2018**, *74*, 2239.; c) X. Yin, J. Z. Low, K. J. Fallon, D. W. Paley, L. M. Campos, *Chem. Sci.* **2019**, *10*, 10733.; d) Y. Ishigaki, Y. Hayashi, T. Suzuki, *J. Am. Chem. Soc.* **2019**, *141*, 18293.; e) Y. Ishigaki, T. Hashimoto, K. Sugawara, S. Suzuki, T. Suzuki, *Angew. Chem. Int. Ed.* **2020**, *59*, 6581.; f) T. Nishiuchi, R. Ito, E. Stratmann, T. Kubo, *J. Org. Chem.* **2020**, *85*, 179.; g) K. Li, Z. Xu, J. Xu, T. Weng, X. Chen, S. Sato, J. Wu, Z. Sun, *J. Am. Chem. Soc.* **2021**, *143*, 20419.

[6]   Typical examples for bianthrones, see: a) H. Meyer, *Ber. Dtsch. Chem. Ges. B.* **1909**, *42*, 143.; b) H. Meyer, *Monatsh. Chem.* **1909**, 30, 165.; c) Y. Taouhi, O. Kalisky, I. Agranat, *J. Org. Chem.* **1979**, *44*, 1949.; d) Y. Hirao, Y. Hamamoto, N. Nagamachi, T. Kubo, *Phys. Chem. Chem. Phys.* **2019**, *21*, 12209.; e) Y. Hamamoto, Y. Hirao, T. Kubo, *J. Phys. Chem. Lett.* **2021**, *12*, 4729.

[7]   a) N. Assadi, S. Pogodin, S. Cohen, I. Agranat, *Struct. Chem.* **2015**, *26*, 319.; b) N. Assadi, S. Pogodin, S. Cohen, I. Agranat, *Asian. J. Org. Chem*. **2015**, *4*, 1392.

[8]   T. Nishiuchi, S. Aibara, T. Kubo, *Angew. Chem. Int. Ed.* **2018**, *57*, 16516.

[9]   Typical reviews for aggregation-induced emission, see: a) J. Mei, N. L. C. Leung, R. T. K. Kwok, J.W. Y. Lam, B. Z. Tang, *Chem. Rev.* **2015**, *115*, 11718.; b) Y. Xie, Z. Li, *Chem. Asian. J.* **2019**, *14*, 2524.; c) Z. Zhao, H. Zhang, J. W. Y. Lam, B. Z. Tang, *Angew. Chem. Int. Ed.* **2020**, *59*, 9888.; d) X. Cai, B. Liu, *Angew. Chem. Int. Ed.* **2020**, *59*, 9868.

[10]   Although **1**-AD also has an anthrone-anthrone π-π interaction, the magnitude of the longer wavelength shift in the $S_0 \rightarrow S_1$ transition (Monomer: 573 nm, Dimer: 578 nm) is smaller than that of **1**-TCE.

[11] Examples of recent mechanochromic molecules, see; a) H. Ito, M. Muromoto, S. Kurenuma, S. Ishizuka, N. Kitamura, H. Sato, T. Seki, *Nat. Commun.* **2013**, *4*, 2009.; b) T. Seki, K. Sakurada, H. Ito. *Angew. Chem. Int. Ed.* **2013**, *52*, 12828.; c) S. Suzuki, R. Maya, Y. Uchida, T. Naota, *ACS Omega,* **2019**, *4*, 10031.; d) Y. Ishigaki, K. Sugawara, M. Yoshida, M. Kato, T. Suzuki, *Bull. Chem. Soc. Jpn.* **2019**, *92*, 1211.; e) T. Nishiuchi, K. Kisaka, T. Kubo, *Angew. Chem. Int. Ed.* **2020**, *60*, 5400.; f) Y. Tani, M. Komura, T. Ogawa, *Chem. Commun.* **2020**, *56*, 6810.

[12] Examples of hydrostatic pressure induced chromism, see: a) K. Nagura, S. Saito, H. Yusa, H. Yamawaki, H. Fujihisa, H. Sato, Y. Shimoikeda, S. Yamaguchi, *J. Am. Chem. Soc.* **2013**, *135*, 10322.; b) Q. Sui, X. –T. Ren, Y. –Z. Dai, K. Wang, W. –T. Li, T. Gong, J. –J. Fang, B. Zou, E. –Q. Gao, L. Wang, *Chem. Sci.* **2017**, *8*, 2758.; c) B. Yu, Y. Wang, L. Wang, X. Tan, Y. –M. Zhang, K. Wang, M. Li, B. Zou, S. X. –A. Zhang, *Phys. Chem. Chem. Phys.* **2019**, *21*, 17696.; d) Q. Sui, P. Li, R. Sun, Y. –H. Fang, L. Wang, B. –W. Wang, E. –Q. Gao, S. Gao, *J. Phys. Chem. Lett.* **2020**, *11*, 9282.; e) D. Zhao, M. Wang, G. Xiao, B. Zou, *J. Phys. Chem. Lett.* **2020**, *11*, 7297.

[13] Examples of reversible thermochromic molecules, see; a) Y. Morita, S. Suzuki, K. Fukui, S. Nakazawa, H. Kitagawa, H. Kishida, H. Okamoto, A. Naito, A. Sekine, Y. Ohashi, M. Shiro, K. Sasaki, K. Sato, T. Takui, K. Nakasuji, *Nat. Mater.* **2008**, *7*, 48.; b) S. Perruchas, C. Tard, X. F. L. Goff, A. Fargues, A. Garcia, S. Kahlal, J. –Y. Saillard, T. Gacoin, J. –P. Boilot, *Inorg. Chem.* **2011**, *50*, 10682.; c) K. Shimada, A. Kobayashi, Y. Ono, H. Ohara, T. Hasegawa, T. Taketsugu, E. Sakuda, S. Akagi, N. Kitamura, M. Kato, *J. Phys. Chem. C*. **2016**, *120*, 16002.; d) T. Nishiuchi, H. Sotome, R. Fukuuchi, K. Kamada, H. Miyasaka, T. Kubo, *Aggregate*, **2021**, *2*, e126.

[14] Upon heating **2**-Y from 140 to 160 °C below the melting point (mp: 163-165 °C) and then standing for several minutes, a single-crystal-to-single-crystal (SCSC) transition to **2**-O begins (Figure S27). Thus, X-ray crystallographic analysis of **2**-Y over 140 °C could not be performed. This thermal induced SCSC transition is a known phenomenon in several organic compounds, see; a) F. H. Herbstein, *Acta. Crystallogr. Sect. B. Struct. Sci.* **2006**, *62*, 341.; b) X. Luo, J. Li, C. Li, L. Heng, Y. Q. Dong, Z. Liu, Z. Bo, B. Z. Tang, *Adv. Mater.* **2011**, *23*, 3261.; c) Y. Abe, S. Karasawa, N. Koga, *Chem. Eur. J.* **2012**, *18*, 15038.

[15] Crystal void volume in a unit cell was calculated by CrystalExplorer program (version 21.5), P. R. Spackman, M. J. Turner, J. J. McKinnon, S. K. Wolff, D. J. Grimwood, D. Jayatilaka, M. A. Spackman, *J. Appl. Cryst.* **2021**, *54*, 1006.

[16] Reversible SCSC transition accompanied with thermochromic fluorescence behaviour was reported, see; S. Yang, P.-A. Yin, L, Li, Q. Peng, X. Gu, G. Gao, J. You, B. Z. Tang, *Angew. Chem. Int. Ed.* **2020**, *59*, 10136.

[17] Examples of force-responsive materials, see; (a) M. K. Beyer, H. C-. Schaumann, *Chem. Rev.* **2005**, *105*, 2921.; (b) M. M. Caruso, D. A. Davis, Q. Shen, S. A. Odom, N. R. Sottos, S. R. White, J. S. Moore, *Chem. Rev.* **2009**, *109*, 5755.; (c) A. L. Black, J. M. Lenhardt, S. L. Craig, *J. Mater. Chem.* **2011**, *21*, 1655.; (d) J. R-. Arino, D. Mark, *Chem. Rev.* **2012**, *112*, 5412.; (e) J. Li, C. Nagamani, J. S. Moore, *Acc. Chem. Res.* **2015**, *48*, 2181.; (f) Y. Liu, K. Galior, V. P-. Y. Ma, K. Salaita, *Acc. Chem. Res.* **2017**, *50*, 2915.; (g) N. W-. Fox, E. Rognin, T. A. Aljohani, R. Daly, *Chem* **2018**, *4*, 2499.; (h) J. M. Brockman, A. T. Blanchard, V. P-. Y. Ma, W. D. Derricotte, Y. Zhang, M. E. Fay, W. A. Lam, F. A. Evangelista, A. L. Mattheyses, K. Salaita, *Nat. Methods* **2018**, *15*, 115.; (i) R. Kotani, S.

Yokoyama, S. Nobusue, S. Yamaguchi, A. Osuka, H. Yabu, S. Saito, *Nat. Commun.* **2022**, *13*, 303.